Sheffield Hallam University

Personalised parameter estimation of the cardiovascular system: Leveraging data assimilation and sensitivity analysis

SAXTON, Harry <http://orcid.org/0000-0001-7433-6154>, SCHENKEL, Torsten <http://orcid.org/0000-0001-5560-1872>, HALLIDAY, Ian <http://orcid.org/0000-0003-1840-6132> and XU, Xu <http://orcid.org/0000-0002-9721-9054>

Available from Sheffield Hallam University Research Archive (SHURA) at:

https://shura.shu.ac.uk/32608/

This document is the Published Version [VoR]

Citation:

SAXTON, Harry, SCHENKEL, Torsten, HALLIDAY, Ian and XU, Xu (2023). Personalised parameter estimation of the cardiovascular system: Leveraging data assimilation and sensitivity analysis. Journal of Computational Science, 74: 102158. [Article]

Copyright and re-use policy

See http://shura.shu.ac.uk/information.html

Sheffield Hallam University Research Archive
http://shura.shu.ac.uk

Journal of Computational Science 74 (2023) 102158

Contents lists available at ScienceDirect

Journal of Computational Science

journal homepage: www.elsevier.com/locate/jocs

Personalised parameter estimation of the cardiovascular system: Leveraging data assimilation and sensitivity analysis

Harry Saxton [a,*], Torsten Schenkel [b], Ian Halliday [c], Xu Xu [d]

[a] Materials & Engineering Research Institute, Sheffield Hallam University, Howard Street, Sheffield, S1 1WB, United Kingdom
[b] Department of Engineering and Mathematics, Sheffield Hallam University, Howard Street, Sheffield, S1 1WB, United Kingdom
[c] Department of Infection, Immunity and Cardiovascular Disease, University of Sheffield, The Medical School, Beech Hill Road, Sheffield, S10 2RX, United Kingdom
[d] Department of Computer Science, University of Sheffield, Sheffield, S1 4DP, United Kingdom

ARTICLE INFO

Keywords:
Data assimilation
Dynamical systems
Uncertainty quantification
Parameter estimation

ABSTRACT

Detailed models of dynamical systems used in the life sciences may include hundreds of state variables and many input parameters, often with physical meanings. Therefore, efficient and unique input parameter identification, from experimental data, is an essential but challenging task for this class of models. This study presents a comprehensive analysis of a nine-dimensional single ventricle lumped-parameter model, representing the systemic circulation. This model is formulated in terms of differential algebraic equations, often found in other areas of the life sciences. We introduce a novel computational algorithm designed to incorporate patient-specific beat-to-beat variability into model investigations, utilising the Unscented Kalman Filter (UKF) for efficient parameter estimation. Our findings demonstrate the exceptional adaptability of the UKF to severe parameter perturbations, representing significant physiological changes. Furthermore, we provide novel insights into the continuous sensitivity of model input parameters, illustrating the robustness and efficacy of UKF. The monitoring of a patient's physiological state, with minimal delay, becomes feasible, by incorporating patient-specific measurements and leveraging the UKF. The workflow presented in this paper enables prompt identification of pathophysiological conditions and will improve patient care.

1. Introduction

Mechanistic models of the cardiovascular system (CVS) can accurately represent patient physiology when supplied with estimated input parameters from clinical data. Lumped parameter models (LPMs) are widely used to assess global haemodynamics [1,2]. These LPMs combine low-order sub-models to describe haemodynamic effects using passive electrical analogues: resistors for flow dissipation, capacitors for organ compliance, and inductors for flow inertial effects. Each component in a cardiovascular LPM corresponds to distinct physiology [1,2]. LPMs, typically 0D, can be coupled with 1D and 3D fluid models, facilitating applications like surgical planning [3,4]. They are used to investigate conditions including pulmonary hypertension, atrial fibrillation, single ventricle physiology, and fetal circulation [5–11].

CV LPMs are valuable in applications involving time-varying input parameters. The incorporation of time-varying input parameters provides important insights into the adaptive nature of the CV system. Accounting for time variation of input parameters allows clinicians and researchers to study CV dynamics and system response to changing conditions. Here, a notable application is CV adaptation to blood volume shifts. For instance, in the context of a head-up tilt test, performed to diagnose orthostatic intolerance [12], time-varying models can simulate blood mis-allocation caused by the dynamic changes in gravitational head associated with posture, which enables clinicians to test hypotheses.

One seeks to personalise LPM models to achieve clinical impact [13] using input parameters which are biomarkers of patient (patho)physiology, which may be used to stratify cohorts or support clinician decisions. Some LPM input parameters may be estimated from clinical measurements, such that the discrepancies between the model outputs and the measurements are minimised. This personalisaiton process (formally, a solution of the inverse operation of the model) is challenging, particularly when the number of input parameters to be estimated is large. LPM input parameters are typically personalised by minimisation of an L_2 norm of some weighted difference between measured (often very noisy and self-inconsistent) target patient data and a corresponding model prediction [14–16]. A LPM model's cost function level-set is

* Corresponding author.
E-mail address: c1050449@hallam.shu.ac.uk (H. Saxton).

https://doi.org/10.1016/j.jocs.2023.102158
Received 30 June 2023; Received in revised form 11 September 2023; Accepted 9 October 2023
Available online 28 October 2023
1877-7503/© 2023 The Author(s). Published by Elsevier B.V. This is an open access article under the CC BY license (http://creativecommons.org/licenses/by/4.0/).

a hyper-surface in the model's input parameter space (which has a dimension equal to the number of input parameters), and personalisation amounts to an attempt to locate its global minimum.

To personalise a model, one investigates the sensitivity of input parameters to specific output metrics. Sensitivity analysis (SA) studies how a change in a model's (often discrete) output can be apportioned to different sources of uncertainty among many input parameters [17]. Two types of SA exist: (i) local SA addresses sensitivity relative to changes in a single input parameter value, varied one at a time, about a fixed operating point, and (ii) global SA examines sensitivity over the entire parameter distribution [18]. For personalised medicine, it is considered essential to examine the whole parameter space [19]. SA can reveal influential parameters in sets, where the members all have similar effects across surveyed outputs. When an input parameter strongly impacts the model outputs, it is deemed identifiable, i.e., it can be uniquely identified for the patient to whom the target data applies. Discrete clinical measurements like stroke volume (SV), mean arterial pressure (MAP), and cardiac output (CO), are commonly used in LPM models, to investigate the effects of input parameters [20–22]. Continuous, possibly invasive measurements, like arterial and ventricular pressure, volume, and flow, are also used.

There is a growing trend towards utilising data assimilation methods (DA) to estimate personalised input parameters of models. While DA methods do not provide a direct metric for assessing the influence of input parameters, they have demonstrated effectiveness in recovering input parameters from experimental data [23]. This stems from their ability to leverage full time-varying measurements. DA has been successfully applied to various CV problems, including the estimation of Windkessel input parameters [24,25] and closed-loop models of single ventricle physiology [26]. Here, our focus lies on the Unscented Kalman Filter (UKF) [27], primarily due to its ability to handle the non-linearities introduced by the valvular and ventricle functions of the LPM.

Conventional LPM models often assume a constant heart rate, which does not accurately reflect CV system dynamics [28]. To address this limitation, Pant et al. [26] proposed a method to estimate model parameters with two varying heart rates, by employing two UKFs in parallel. However, there is currently a gap in the literature regarding the inclusion of personalised heart rate measurements, which are easily obtainable in a clinical setting [29]. When investigating time-varying parameters, Matzuka et al. [30] utilised the Ensemble Kalman Filter to estimate input parameters involved in baro-reflex regulation. Matzuka's approach incorporates the inherent time-varying nature of the parameters, due to the model's embedded physics. If LPMs are to be integrated into clinical workflows, they must be able to adapt perturbations to their dynamics that originate outside the model. For instance, during a medical procedure, suppose there is a drop in arterial compliance or vascular resistance; the UKF should be able to re-calibrate to this change, based upon a feed of patient data and then provide the clinician with re-estimated input parameters, that accurately represent the patient's evolving physiological state.

Here, we take an established generic differential equation model of the systemic circulation, and layer-on a novel approach to integrate patient-specific heart rate measurements into it. We evaluate the sensitivity of the model input parameters and explore the continuous outputs. We utilise synthetic, noisy data representative of patient scenarios to evaluate the accuracy of input parameters recovered using the UKF. Additionally, we assess our UKF's robustness by perturbing our base model's input parameters, to represent severe changes in a patient's physiological state. Finally, we discuss the potential integration of our method into a clinical workflow.

The structure of this paper is as follows. Section 2 provides a detailed explanation of the methods and implementation used in this study. In Section 3, we present the results obtained from our analysis. Finally, in Section 4, we provide a comprehensive comparison and discussion of the optimal sets of input parameters obtained through our proposed methods.

2. Methods

In Section 2.1, we describe the single ventricle model formulated as differential algebraic equations. It is used to simulate the systemic circulation in this work. In Section 2.2 we explain how we modify the computational model to include patient-specific heart rates, on a beat-to-beat basis. We then detail how realistic synthetic patient data are generated and how input parameters are perturbed to test the robustness and efficiency of the UKF, in Section 2.3. In Section 2.4, we explain how both continuous and time averaged SA is used to analyse the single ventricle model. The UKF is described in Section 2.5, where we pay particular attention to how representative patient data are incorporated into the computational algorithm.

All computation was performed using Julia[1] [31], employing packages DifferentialEquations.jl [32], GlobalSensitivity.jl [33] and QuasiMonteCarlo.jl to solve the dynamical systems, calculate the sensitivity indices and sample input parameter space. Specifically, simulations were solved using Rodas5 algorithm [34], with relative and absolute tolerances set to 10^{-8}. We used a fixed time step of $dt = 0.0005$ s and 15 cardiac cycle times were generated. We implemented parameter perturbations from $t \geq 8$ s. To compute the continuous sensitivity analysis, we analysed cycles 10 to 13 at a constant time step of 0.0005s to ensure sufficient accuracy. We used Makie.jl to visualise results [35].

2.1. Single ventricle model

Given a dynamical system has the generic form:

$$\frac{d}{dt}\underline{X}(t;\underline{\theta}) = \underline{f}\left(\underline{X}(t;\underline{\theta});\underline{\theta}\right), \quad \underline{Y}(t;\underline{\theta}) = \underline{h}(\underline{X}(t;\underline{\theta})), \tag{1}$$

where $\underline{X}$, $\underline{Y}$, $\underline{f}$, $\underline{\theta}$ and $\underline{h}$ represent the state variable vector, the output vector, the dynamical system functions, the input parameter vector and the measurement operator, respectively.

We study a three-compartment system-level, ordinary differential equation based, electrical analogue cardiovascular model, after Bjordalsbakke et al. [22] (see Fig. 1). The state of each compartment is specified by its time-dependant dynamic pressure P (mmHg), an inlet flow Q (mL/s) and a volume V (mL):

$$X_i(t) = \left(V_i(t), P_i(t), Q_i(t)\right), \quad i \in \{lv, sa, sv\}, \tag{2}$$

where lv denotes the left ventricle, sa the systemic arteries and sv the venous system. Formally, t is a continuous variable.

The equations relating to the passive compartmental state variables take the following forms:

$$\frac{dV_{s,i}}{dt} = Q_i - Q_{i+1}, \quad \frac{dP_i}{dt} = \frac{1}{C_i}(Q_i - Q_{i+1}), \quad Q_i = \frac{P_i - P_{i+1}}{R_i}, \tag{3}$$

where the subscripts $(i-1), i, (i+1)$ represent the proximal, present and distal system compartments, respectively. $V_{s,i}$ (mL) denotes the circulating (stressed) volume [36], C_i (ml/mmHg) and R_i (mmHgs/mL) denote compartmental compliance and the Ohmic resistance between compartments i and $(i+1)$. See Fig. 1 and Table 1.

In Fig. 1, we use a C-R-C Windkessel [37] to represent the systemic circulation. The flow in and out of the active left ventricle is controlled by the mitral and aortic valves, respectively. The valves are modelled as diodes, with Ohmic resistance under forward bias and infinite resistance under reverse bias:

$$Q_i = \begin{cases} \frac{P_i - P_{i+1}}{R_{val}}, & P_i > P_{i+1}, \\ 0 & P_i \leq P_{i+1}, \end{cases} \tag{4}$$

where R_{val} represents the resistance across the respective valves.

Let us consider the active model compartment. The dynamics of the left ventricle is described by a time-varying compliance $C(t)$, or elastance, $E(t)$ (mmHg/ml) (elastance is the reciprocal of compliance)

[1] Code is available at https://github.com/H-Sax/UKF_SpecialEdition

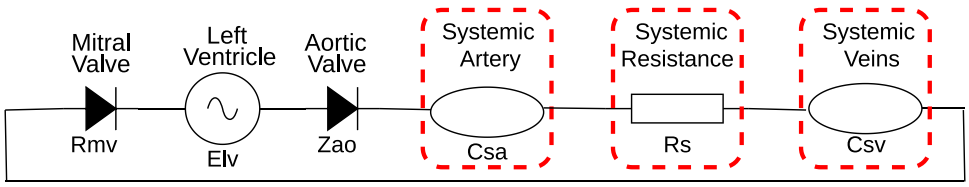

Fig. 1. Schematic representation of both the simple and advanced electrical analogue models utilised in this work. The system is a nine parameter representation of the systemic circulation, originally presented by Bjordalsbakke et al. [22].

Table 1
Model input parameters.

Parameter θ (units)	Description	Initial value
E_{max} $\left[\frac{\text{mmHg}}{\text{ml}}\right]$	Maximal ventricular contractility	1.5
E_{min} $\left[\frac{\text{mmHg}}{\text{ml}}\right]$	Minimal ventricular contractility	0.03
τ_{es} (s)	End systolic time	0.3
τ_{ep} (s)	End pulse time	0.45
Z_{ao} $\left[\frac{\text{mmHg s}}{\text{ml}}\right]$	Aortic valve resistance	0.033
R_{mv} $\left[\frac{\text{mmHg s}}{\text{ml}}\right]$	Mitral valve resistance	0.06
R_s $\left[\frac{\text{mmHg s}}{\text{ml}}\right]$	Systemic resistance	1.11
C_{sa} $\left[\frac{\text{ml}}{\text{mmHg}}\right]$	Systemic compliance	1.13
C_{sv} $\left[\frac{\text{ml}}{\text{mmHg}}\right]$	Venous compliance	11.0

Each input parameter's unit is stated alongside a chosen initial value for the simplified systemic circulation model. τ is the cardiac cycle length, which is fixed such that $\tau = 1$ s. The ventricular shift parameter $E_{\text{shift}} = 0$ (s) as no atrium is present in the simplified 9 parameter model.

which determines the change in pressure for a given change in the volume [36]:

$$E_{lv}(t) = \frac{P_{lv}(t)}{V_{lv}(t) - V_0} = \frac{P_{lv}(t)}{V_{lv,s}(t)}, \tag{5}$$

where V_0 & $V_{lv,s}(t)$ represent the unstressed and stressed volumes in the left ventricle, respectively. $E(t)$ may be described in an analytical form as follows [38]:

$$E(t) = (E_{max} - E_{min}) \cdot e(t) + E_{min},$$
$$e(t) = \begin{cases} \frac{1}{2}(1 - \cos(\frac{\pi t}{\tau_{es}})), & 0 \le t < \tau_{es}, \\ \frac{1}{2}(1 + \cos(\frac{\pi(t-\tau_{es})}{\tau_{ep}-\tau_{es}})), & \tau_{es} \le t < \tau_{ep}, \\ 0, & \tau_{ep} \le t < \tau, \end{cases} \tag{6}$$

where $e(t; \tau_{es}, \tau_{ep})$ is the activation function for both the ventricle, which is parameterised by the end systolic and end pulse timing parameters τ_{es} and τ_{ep} respectively. Computationally, the time step is updated as: $t = (t + (1 - E_{shift}) * \tau) \text{mod } \tau$.

The elastance function is defined over one cardiac cycle, i.e., time $t \in [0, \tau]$ with τ being the length of the cardiac cycle. τ is often fixed as 1 second which is not physiologically realistic: we return to this issue in Section 2.2. The time shift parameter E_{shift} controls when $e(t)$ is activated. E_{shift} is fixed at 0 for the left ventricle. Maximal contractility, E_{max}, and minimal contractility, E_{min}, both control the left ventricular elastance extrema.

2.2. Personalised cardiac cycle length

In the clinic, a personalised cardiac cycle length time is obtained non-invasively [29]- heart rate (HR) is an intuitive measurement of a patient's physiological state, from which one obtains the cardiac cycle time length as:

$$\tau = \frac{60}{\text{HR}} \tag{7}$$

with HRis measured in BPM and τ can vary from heartbeat to heartbeat (Heart Rate Variability, HRV). This means that the active chamber elastance equations, defined in Eq. (6) change between each CV cycle. While these measurements are taken from a patient in the clinic, we synthesise cardiac cycle lengths as

$$\tau_i \sim U(0.8, 1.1), \ i = 1, \dots, n, \tag{8}$$

where τ_i represents the cardiac cycle length at cycle i. Above, U denotes the uniform distribution. We construct and simulate an n-dimensional vector $t_{\tau,n}$, of cumulative times such that the vector satisfies the property

$$t_{\tau,n} = \sum_{i=1}^{n} \tau_i. \tag{9}$$

To implement the algorithm we define a global variable τ to represent the cycle time length at a cycle i. We further define a global variable t_r which represents a reset time for which the active chamber is to begin its cardiac cycle again. The cardiac cycle is made up of three distinct phases: systole, diastole and passive filling. With this algorithm, it is assumed that the passive filling phase is reduced and the distinct phases of systole and diastole will occur. The varying cardiac cycle lengths are implemented as a callback such that when the condition is satisfied: integrator.$t - t_r > \tau$, w here integrator.t is the internal time variable of the differential equation solver. We then find the new cardiac cycle time such that

$$\tau = t_{\tau,i+1} - t_{\tau,i} \tag{10}$$

and the reset time becomes

$$t_r = t_{\tau,i}. \tag{11}$$

In Eq. (6), the internal time variable t becomes

$$t = t - t_r. \tag{12}$$

Implementing Eq. (11) is a vital step which informs the elastance to reset at the previous cardiac cycle length, τ_i and is defined over the new cardiac cycle length. For specific implementation guidance, please visit the code for this work at https://github.com/H-Sax/UKF_SpecialEdition.

In reality, the personalised HR would not act in such a random manner, it is more likely to either monotonically increase or decrease. Therefore implementing HR in this way allows us to cope with a worst case scenario, facilitating a more stringent test of the UKF than in a clinical setting.

2.3. Parameter perturbations & synthetic data

We derive noisy synthetic patient waveform data from forward model solutions characterised (note, for nominally true parameter values) for lv pressure P_{lv}, lv volume V_{lv} and systemic pressure P_{sa} for 15 cycles, representing continuous clinical measurements from (say) echocardiography for V_{lv} [39] and arterial line measurement for P_{sa} [40] (Cardiac catheterisation can be performed to extract P_{lv} [41]). To align with the purpose of a UKF our forward numerical solutions are subject to multiplicative Gaussian corruption as follows:

$$\underline{Y}_j^m = \underline{h}(\underline{X}(t_j, \underline{\theta}_t)), \qquad \underline{Y}_j^n = \underline{h}(\underline{X}(t_j, \underline{\theta}_t)) \cdot (1 + \psi_j). \tag{13}$$

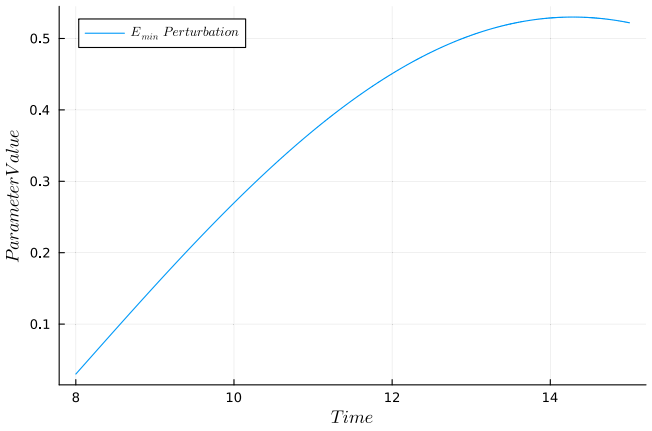

Fig. 2. Parameter Perturbation - We show the perturbation applied to the minimal contractility parameter E_{min}. From $t > 8$, the perturbation becomes positive, demonstrating an increase in minimal ventricular contractility.

Above, the subscript j denotes sampling time, deemed to be the discrete time of the numerical solution, superscript n indicates a noisy solution and superscript m denotes the measured, un-corrupted numerical solution. ψ_j is an independent, normally-distributed random variable, with zero mean and a standard deviation 0.025, which is typical [25].

We propose two types of perturbation to the input parameters applied from $t > 8$ (having run the model to steady state) until the end cycle. The first perturbation we apply is to the timing parameters of the active chamber parameters, such that for every cycle $t > 8$ we apply a random value for τ_{es} and τ_{ep} satisfying the distributions

$$\tau_{es} \sim N(0.3, 0.03^2), \ \ \tau_{ep} \sim N(0.45, 0.03^2). \tag{14}$$

The second parameter perturbation applied to the non-timing parameters of the model describes a gradual increase from $t > 8$ and is represented in Fig. 2 and Eq. (15):

$$p(t) = \frac{1}{2}\sin\left(\frac{t - t_0}{4}\right) + p_0, \tag{15}$$

where $p(t)$ represents the value of an input parameter (see Table 1) at time t. t_0 represents the time at which the perturbation is applied. $t_0 = 8$. p_0 represents the true value of the input parameter, before it is perturbed, i.e., for E_{min}, $p_0 = 0.03$.

2.4. Sensitivity analysis

Consider discrete outputs: $Y_i = Y(t_i)$. In our model setting, these outputs are normally clinical measurements like SV, MAP and CO. Y_i is determined by the values of input parameters, which are assumed to be continuously distributed over some physiological range, so one can view the $Y_i = Y(t_i)$ as integrable multivariate functions. A variance-based approach is employed to calculate the first-order or total-order effect of a generic input parameter θ_i. The complementary set, denoted as θ_i^c, refers to all other model inputs excluding θ_i. The first-order sensitivity index is:

$$S_i = \mathrm{Var}_{\theta_i}(E_{\theta_i^c}(Y|\theta_i)), \tag{16}$$

where E represents the expectation operator. The inner expectation operator determines the mean of Y across all possible values of θ_i^c, keeping θ_i fixed. The outer variance considers all possible values of θ_i. In the sequel, we will utilise the identity [42]:

$$\mathrm{Var}_{\theta_i}(E_{\theta_i^c}(Y|\theta_i)) + E_{\theta_i}(\mathrm{Var}_{\theta_i^c}(Y|\theta_i)) = \mathrm{Var}(Y), \tag{17}$$

where $\mathrm{Var}_{\theta_i}(E_{\theta_i^c}(Y|\theta_i))$ quantifies the first-order (additive) effects of θ_i on the model outputs.

Another commonly used measure of variance is the total-order estimator, initially introduced by Homma [43]:

$$S_{T,i} = E_{\theta_i^c}(\mathrm{Var}_{\theta_i}(Y|\theta_i^c)) = \mathrm{Var}(Y) - \mathrm{Var}_{\theta_i^c}(E_{\theta_i}(Y|\theta_i^c)), \tag{18}$$

where $S_{T,i}$ captures the total effect of both the first-order effects and higher-order effects (multiplicative interactions) of the input parameter θ_i. This can be understood by recognising that $\mathrm{Var}_{\theta_i^c}(E_{\theta_i}(Y|\theta_i^c))$ represents the first-order effect of θ_i^c. Therefore, $\mathrm{Var}(Y) - \mathrm{Var}_{\theta_i^c}(E_{\theta_i}(Y|\theta_i^c))$ accounts for the contribution of all terms in the variance decomposition that include the input θ_i. The equations can be derived by utilising a Hoeffding-Sobol decomposition, and utilising the fact that each term is assumed to be square-integrable. See e.g. [44,45].

Let us consider continuous measurements such as arterial pressure and ventricular pressure. Eck et al. [46] addressed the limitation of the scalar sensitivity indices (Eqs. (16) and (18)) in partitioning the variability of non-scalar quantities of interest. If one desires discrete indices for time varying outputs, a new method is required. As the variance is not constant over time, comparing the sensitivity indices of input parameters at two different time points becomes challenging in terms of quantifying the total uncertainty contributed by a specific parameter. Hence, the sensitivity coefficients (locally scaled) at two points in time are not directly comparable, in terms of the total uncertainty contributed by a given parameter. To overcome this issue, these authors introduced what is known as time averaged sensitivity indices:

$$S_{[1,T],i} \to \frac{\sum_k S_{[1,T],i}\mathrm{Var}(\underline{Y}(t_k))}{\sum_k \mathrm{Var}(\underline{Y}(t_k))}, \tag{19}$$

where S_1 represents the first-order indices which inform on relative influence of every input (total order indices, S_T, inform on relative influence of every input parameters interactions with others). $\underline{Y}$ denotes the measured model continuous outputs and i identifies the particular input parameter whose sensitivity is at issue. We are still interested in how the sensitivity indices vary between two time points and so define the sensitivity indices

$$S_{[1,T],i} \to S_{[1,T],i}\mathrm{Var}(\underline{Y}(t_k)) \tag{20}$$

This metric then defines the sensitivity of an input parameter between two time points, which allows us to evaluate the change in influence during a cardiac cycle, given the presence of beat-to-beat variation.

2.5. Unscented Kalman filter

The UKF is a data assimilation method to unify model results with available measurements, to provide an improved estimation of a dynamical system [47] states and parameters. The UKF consists of two distinct steps, firstly the unscented transform (UT) calculates the statistics of an assumed Gaussian random variable that undergoes a non-linear transformation [48]. Both multiplicative and additive noise has been investigated with UKF, we assume additive noise throughout the whole model, which is accepted practice for biological systems [49–51]. See below for a description with particular attention given to the influence of patient-specific measurements and how this method could be used to create clinical impact.

We generate an augmented vector $\underline{x} = [\underline{X}, \underline{\theta}]$, where $\underline{X}$ and $\underline{\theta}$ are the state variables and input parameters; see (1). We assume that the augmented state vector $\underline{x}$ is a Gaussian random variable (GRV) of dimension L where $L = \dim(\underline{X}) + \dim(\underline{\theta})$. Now consider propagating the augmented state-vector through the non-linear function $\underline{f}$. Here and for most biological systems, the non-linear function is represented by a set of ODEs. We measure P_{lv}, P_{sa}, V_{lv}, $\underline{Y}(t) = \underline{h}(\underline{x}(t))$, where $\underline{h}$ is the previously-identified operator. We acquire the ODE solution to P_{lv}, P_{sa} and V_{lv}. Assume our GRV has a mean $\underline{x}_\mu$ and a covariance $P_{\underline{x}}$. To compute the statistics on the propagation of the GRV through $\underline{f}$, we

construct a matrix $\underline{\underline{\chi}}$ of $2L+1$ sigma vectors χ_i, where i represents the ith column of the matrix according to the following, for $t = 0, \dots, \infty$:

$$\chi_{0,t} = \underline{x}^A_{\mu,t}, \;\; \chi_{i_{1,t}} = \underline{x}^A_{\mu,t} + \left(\sqrt{(L+\lambda)P^A_{\underline{x},t}}\right)_j, \;\; \chi_{i_{2,t}} = \underline{x}^A_{\mu,t} - \left(\sqrt{(L+\lambda)P^A_{\underline{x},t}}\right)_j, \\ i_1 = j = 1, \dots, L, \quad i_2 = L+1, \dots, 2L, \tag{21}$$

where the superscript A represents the assimilated state and parameter vector. The GRV sigma vectors now represent a minimal set of carefully chosen sample points, which completely capture the true mean and covariance of the GRV. When they are propagated through the true non-linear system, the posterior mean and covariance are captured accurately to the 3rd order (Taylor series expansion) for *any* non-linearity. A derivation of the UKF can be found in [52].

Next, we compute a set of corresponding weights W_i:

$$W^\mu_0 = \frac{\lambda}{L+\lambda}, \;\; W^c_0 = \frac{\lambda}{L+\lambda} + (1+\beta-\alpha^2), \;\; W^\mu_i = W^c_i = \frac{1}{2(L+\lambda)}, \\ i = 1, \dots, 2L, \;\; \lambda = \alpha^2(L+\kappa) - L, \tag{22}$$

where λ is a scaling parameter, α determines the spread of sigma points around $\underline{x}_\mu$ (we use $\alpha = 10^{-1}$). κ is another scaling parameter (here $\kappa = 0$) and β incorporate prior knowledge of which distribution $\underline{x}$ follows. Here $\beta = 2$ is used as this is optimal for GRV. The matrix square root is performed using a Cholesky decomposition [53] which requires the matrix to be positive definite.

Next, we propagate each sigma vector through the ODE system such that $Y_i = \underline{f}(\chi_i)$ and determine the mean and covariance of $\underline{Y}$, using the weighted sample mean and covariance of the propagated sigma vectors. Before we can do this, we must first define the prediction step in the algorithm

$$\hat{\chi}_{t+1|t} = \underline{f}(\chi_t), \;\; Y_{t+1|t} = \underline{h}(\hat{\chi}_{t+1|t}). \tag{23}$$

The above have corresponding mean and sample covariance:

$$\underline{x}_{\mu,t+1} = \sum_{i=0}^{2L} W^\mu_i \hat{\chi}_{i,t+1|t}, \\ P_{\underline{x},t+1} = \sum_{i=0}^{2L} W^c_i [\hat{\chi}_{i,t+1|t} - \underline{x}_{\mu,t+1}][\hat{\chi}_{i,t+1|t} - \underline{x}_{\mu,t+1}]^T + \delta_Q I, \\ \underline{Y}^\mu_{t+1} = \sum_{i=0}^{2L} W^\mu_i Y_{i,t+1|t}, \\ P_{\underline{Y},t+1} = \sum_{i=0}^{2L} W^c_i [Y_{i,t+1|t} - \underline{Y}^{\mu,t+1}][Y_{i,t+1|t} - \underline{Y}^{\mu,t+1}]^T + R, \\ P_{\underline{x}\underline{Y},t+1} = \sum_{i=0}^{2L} W^c_i [\hat{\chi}_{i,t+1|t} - \underline{x}_{\mu,t+1}][Y_{i,t+1|t} - \underline{Y}^{\mu,t+1}]^T, \tag{24}$$

where $P_{\underline{x}\underline{Y}}$ is designated the cross correlation matrix. R is the additive noise on the predicted measurements and takes the form $\sigma^2 I_{3\times3}$ (for 3 measurements), where $\sigma = 5$. This represents the typical clinical error present when measuring ventricular/aortic pressure and the ventricular volume [54]. $\delta_Q I$ is considered a regularisation term to avoid sigma point collapse [51,55], where I is an $L \times L$ identity matrix with $\delta_Q = 10^{-8}$.

We now correct the prediction that has been made by assimilating the noisy data generated in Eq. (13). The Kalman gain matrix is calculated as

$$K_{t+1} = P_{\underline{x}\underline{Y},t+1}(P_{\underline{Y},t+1})^{-1},$$

which then leads to:

$$\underline{x}^A_{\mu,t+1} = \underline{x}_{\mu,t+1} + K_{t+1}(\underline{Y}^n_{t+1} - \underline{Y}^\mu_{t+1}), \\ P^A_{\underline{x},t+1} = P_{\underline{x},t+1} - K_{t+1} P_{\underline{Y},t+1} K^T_{t+1}, \tag{25}$$

where $\underline{x}^A_{\mu,t+1}$ and $P^A_{\underline{x},t+1}$ are used to generate new sigma points for the $t+1$ time point. In the assimilation step defined in Eq. (25), $\underline{Y}^n_{t+1}$ represents the data which are specific to a patient. Therefore we are correcting the value parameter/state estimation with the measured patient data (represented by the noisy synthetic data in this case). This also allows us to make predictions about compartments in which experimental data are not available, for example aortic valve resistance Z_{ao}. We defer further exploration of this point to the discussion in Section 4. Given the GRV assumption which is needed for the UKF we must transform the deterministic input parameters specified in Table 1 to the Gaussian setting. Each input is then transformed as

$$\theta^N_i \sim N(\theta_i, \sigma^2_i),$$

where θ^N_i is the normally distributed input parameter i with an initial mean θ_i and variance σ^2_i, respectively. The mean of the normal distribution is taken from the literature values as shown in Table 1 [56]. The parameter variance is selected to reflect the uncertainty in the mean parameter value and taken from existing literature [25,26], where larger variances are specified for input parameters with higher uncertainty. This normal distribution reflects the prior belief about the input parameters before any measurements are incorporated. As the UKF iterates, the mean and variance are updated to reflect information gained from new measurements. The initial distribution seeds the estimation process, providing a starting point that is adjusted as more measurement data become available. The means and standard deviations prescribed for each input parameter based on this approach can be found in Table 2.

Table 2
Normal (Gaussian) distribution parameters of the single ventricle model.

Parameter	θ	σ
τ_{es}	0.3	0.01
τ_{ep}	0.45	0.01
R_{mv}	0.06	0.01
Z_{ao}	0.033	0.01
R_s	1.11	0.3
C_{sa}	1.13	0.3
C_{sv}	11.0	0.3
E_{max}	1.5	0.3
E_{min}	0.03	0.01

θ - Initial mean from [56]. σ - Standard deviation from [25,26].

To implement the UKF, we take advantage of the versatile SciML ecosystem within Julia. Here we implement a discrete callback which performs the Kalman filtration at each time point and returns the corrected result. This has been shown to contribute negligible computational time associated with the callback, which demonstrates our ability to produce the result in close-to-real time. Most authors manually discretise the ODE system to transform it into a discrete time system for the implementation of an UKF. Implementing a callback allows us to take advantage of advanced ODE solvers within package DifferentialEquations.jl with improved accuracy. An important point to note here is that there are two distinct steps in our workflow, (1) we perform a first solve of the dynamical system to generate the synthetic data, including perturbed input parameters along with the synthetically generated personalised HRs. This stage represents experimental data collection. (2) These data are then stored for the second stage, when we solve the model and call the UKF. In this step, we estimate the states and input parameters of the model, given the personalised HRs and perturbed input parameters. The aim is that the algorithm can capture the dynamical effects pf changing input parameters which represent evolving physiological conditions of patients.

To evaluate the effectiveness of the UKF estimation procedure we employ the root mean squared error as found below:

$$RMSE = \sqrt{\frac{(\theta_i - x^A_{\mu,i})^2}{n}}, \tag{26}$$

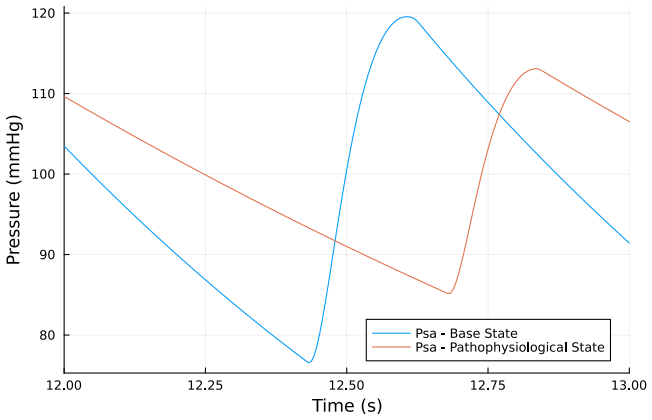

Fig. 3. Systemic arterial pressure - The figure displays the arterial pressure for a base state simulation (blue) and when blood volume is halved and systemic resistance is doubled (orange).

where θ_i is the true value of the ith input parameter, $x^A_{\mu,i}$ is the assimilated estimate of the ith input parameter and n is the length of the assimilated vector. In the case of perturbing the input parameter by the continuous function $p(t)$ found in Eq. (15) θ_i is replaced by $p(t)$ from $t > 8$ which is when the perturbation is applied. This allows us to compare parameter estimates before and after the perturbation. In the case of the timing parameters being perturbed, we compare the assimilated estimate at the start of each cardiac cycle for $t > 8$ to the true perturbed value of the timing parameters and report the average RMSE. The RMSE provides a measure of the average difference between the estimated values and the true values of the input parameters. The input parameter with the lower RMSE value indicates the mot effective estimation as the input parameter aligns more closely to the true value.

3. Results

Within this section, we conduct the continuous sensitivity analysis of our model, examine the UKFs ability to recover input parameters when no perturbations are present and analyse the robustness of the model investigated (Section 3.1). We then examine the ability of UKF to recover true input parameters when they are perturbed from base states (Section 3.2). For each case explored we display a Table of RMSE for each input parameter before and after a perturbation has been applied. The values presented in the Table are accurate to 1sf. All results presented below are discussed in full within Section 4.

3.1. Base state

Fig. 3 displays the case where a patient may be haemorrhaging blood, so blood volume drops and as a consequence, systemic resistance increases in order to maintain arterial pressure (denoted by the orange curve). For the simulation of this situation, initial blood volume was halved and the systemic resistance was doubled. The mean values of the arterial pressure for the base state and the pathophysiological state were 97.8 mmHg and 98.2 mmHg. Given, this case examined is very unlikely to occur in clinic, the model response is in line with expectation providing confidence of the affected model to adapt to other pathophysiological states.

Fig. 4 shows the implementation of the UKF when no parameter perturbations are present- only beat-to-beat variability. Evidently, the input parameters are estimated with remarkable precision from the outset. The only parameter that deviates beyond 1% of its true value is C_{sv}, as depicted in Fig. 4G. Nonetheless, both R_{mv} (Fig. 4C) and R_s (Fig. 4E) exhibit noticeable deviations from their true parameter values, indicated by the yellow line. However, they still demonstrate superior accuracy compared to existing medical devices [57]. Most input parameters exhibit consistent variance, with the exceptions in Figs. 4N, 4P, and 4Q, which correspond partially to the input parameters that were not estimated within 1% accuracy. Notably, certain input parameters, as shown in Figs. 4J, 4K, 4L, 4M, 4O, and 4R, exhibit consistent periodic variation. These input parameters, characterised by steady variance, also demonstrate exceptional accuracy, except for R_{mv} in Fig. 4C. In Table 3 the root mean squared error (RMSE) is displayed for all input parameters. E_{min} displays the smallest RMSE. C_{sv} exhibits RMSE values an order of magnitude larger than the rest of the input parameters. It can be observed that the RMSE decreases by an order of magnitude in the second half of the observed time span.

Table 3
Single ventricle base state RMSE.

Parameter	τ_{es}	τ_{ep}	R_{mv}	Z_{ao}	R_s	C_{sa}	C_{sv}	E_{max}	E_{min}
RMSE $t \leq 8$ s	0.005	0.009	0.005	0.003	0.05	0.01	0.8	0.04	0.003
RMSE $t > 8$ s	0.0005	0.0004	0.002	0.001	0.03	0.02	0.6	0.007	0.0006

The first row shows the RMSE values of input parameters for $t \leq 8$ s. The second row displays the RMSE values of the input parameters for $t > 8$ s.

In Fig. 5, we show the continuous sensitivity of the input parameters where no perturbations are applied with respect to arterial pressure. See Appendix for the sensitivity analysis of input parameters to the other measurements (similar to Fig. 5). We see the sensitivity of input parameters obeys dynamics which mimic a cardiac cycle. We see some parameters, such as τ_{es}, R_{mv}, R_s and C_{sa} in Figs. 5A, C, E, F, exhibit a consistent level of sensitivity during the whole CV cycle with the τ_{es} Fig. 5A being the most influential during the whole cardiac cycle. We see the parameters E_{min}, E_{max}, Z_{ao} and C_{sv} exhibit orders of magnitude change in sensitivity during the cycle. In Fig. 5B we see the end pulse time τ_{ep} appears to have no influence of the arterial pressure during the whole cardiac cycle.

3.2. Parameter perturbations

Here we examine the UKF's ability to estimate input parameters accurately when they are perturbed away from the "baseline" value during each cardiac cycle. We apply the perturbations defined in Eqs. (14) and (15) from $t \geq 8$.

3.2.1. τ_{es} & τ_{ep}

Fig. 6 demonstrates the UKF's ability to adapt to perturbations of the timing parameters τ_{es} and τ_{ep}. The UKF adapts to the perturbed points with exceptional ability as seen in Figs. 6A and 6B. The original parameter values were $\tau_{es} = 0.35$ and $\tau_{ep} = 0.45$, the perturbed values for the cycles were $\tau_{es} = [0.35, 0.27, 0.27, 0.28, 0.34, 0.28, 0.31, 0.26]$ and $\tau_{ep} = [0.43, 0.46, 0.47, 0.44, 0.46, 0.44, 0.43, 0.43]$ to 2dp. The variance of the parameters in Figs. 6J and 6K appear consistent despite the perturbations. Figs. 6I and 6R represent the estimation and variance of the parameter E_{min} respectively. There is disruption to the parameter estimation despite the true value of E_{min} being found during each cardiac cycle. There is minimal disruption to the parameter variance. We see similar behaviour with the aortic valve resistance Zao, and maximal contractility E_{max} in Figs. 6D, 6M, 6H and 6Q respectively. The common theme between both is that the parameter estimations return to the true parameter values during each cardiac cycle. The estimations of all input parameters apart from C_{sv} exhibit minimal errors. The RMSE values in Table 4 indicate that no input parameter estimations suffer from perturbing the timing parameters of the elastance function. Some input parameter estimates improve as the simulation progresses. C_{sv} exhibit the worst RMSE by an order of magnitude when compared to the other input parameter estimates.

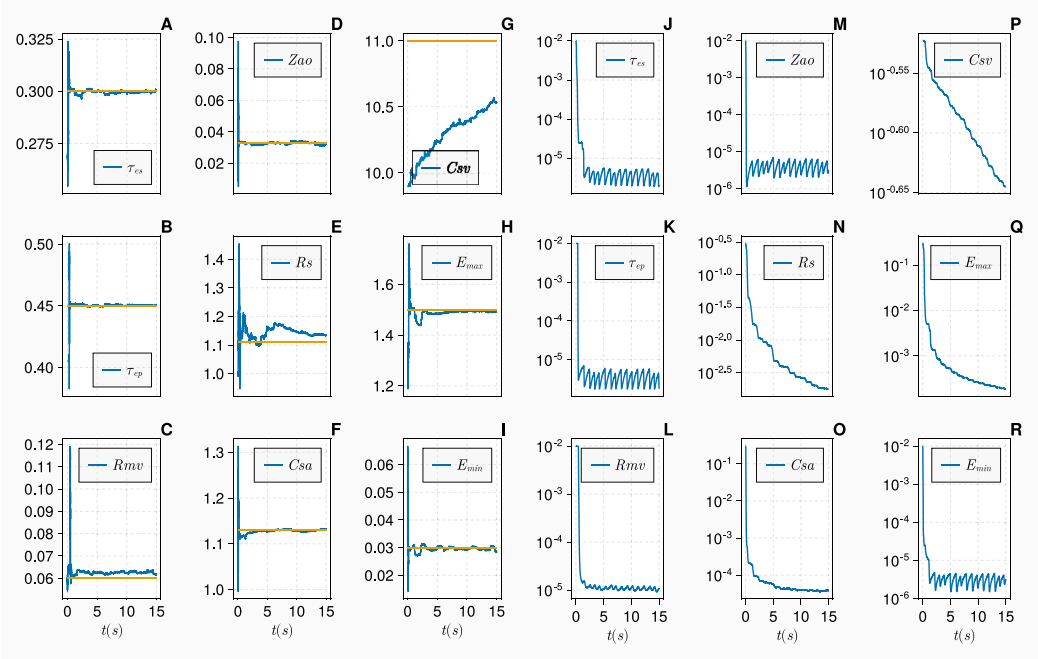

Fig. 4. Single Ventricle Base State Estimation - Figures **A–I** display the parameter estimations over the 15 cardiac cycles. The yellow and blue line represent the true and estimated parameter values respectively. Figures **J–R** display the parameter covariances over the 15 cardiac cycles.

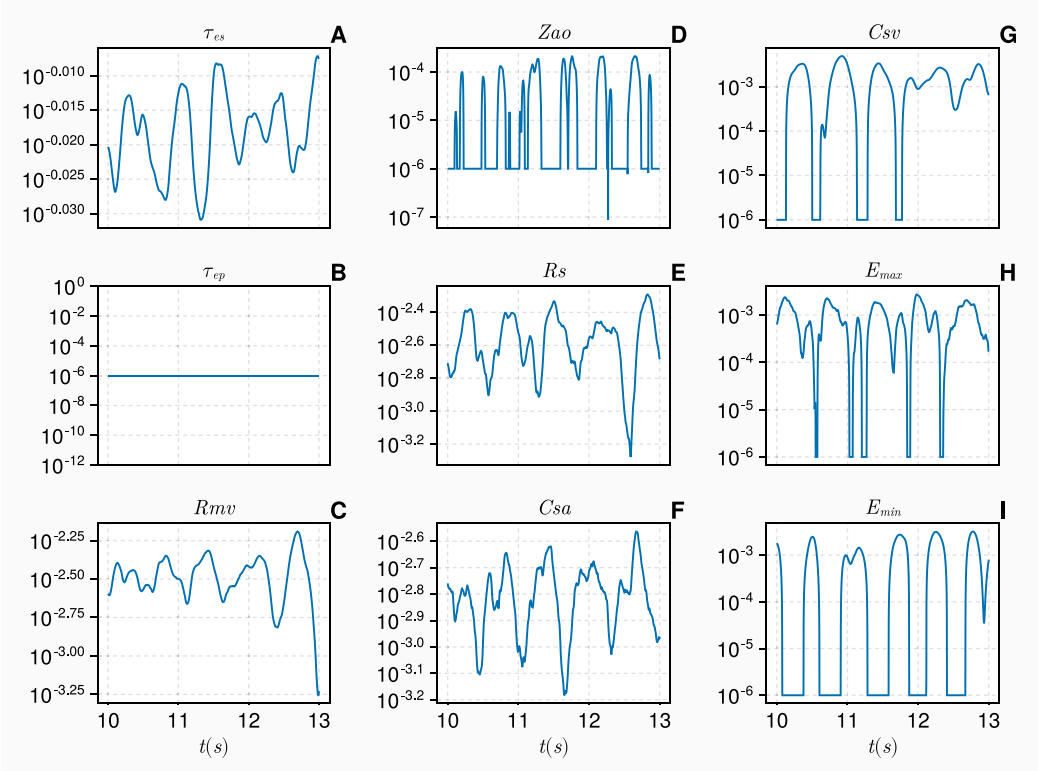

Fig. 5. Single Ventricle Base State Sensitivity - Figures **A–I** display the continuous parameter sensitivities with respect to the arterial pressure. All parameters which returned 0 for sensitivity are set to a value of 10^{-6} in order to plot a log scale.

3.2.2. E_{min}

Fig. 7 demonstrates the UKF's ability to estimate the minimal contractility E_{min} given the perturbation defined in Eq. (15). In Fig. 7I, we see minimal contractility traces the perturbation with excellent accuracy. We see the perturbation also impacts the variance of the parameter, causing a gradual increase, from when it is applied. This increase in parameter variance is also present in other input parameters (where the perturbation is not applied), seen in Figs. 7J, K, L, M, O, R. The timing parameters of the elastance function, τ_{es} and τ_{ep}, appear to diverge from the true parameter values when the perturbation is applied, as seen in Figs. 7A and 7B. We observe all input parameter estimates returns to the true parameter value by the final cycle at

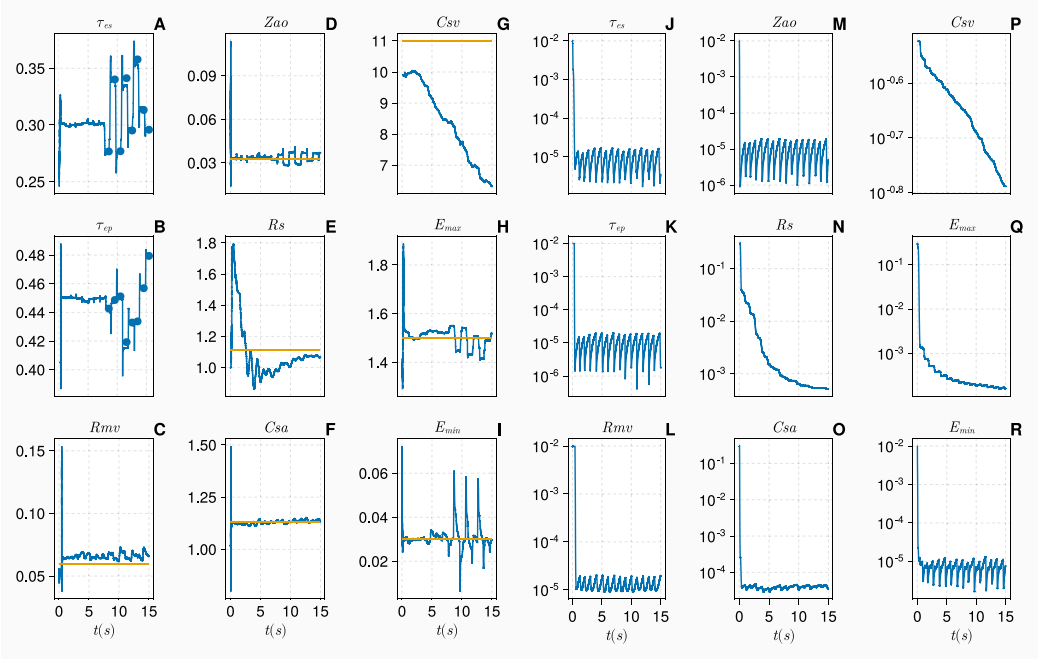

Fig. 6. τ_{es} & τ_{ep} - Figures **A–I** display parameter estimations over 15 cardiac cycles with varying values for τ_{es} and τ_{ep}. The yellow and blue line represent the true and estimated parameter values respectively, the blue dots represent the perturbed values on the input parameters. Figures **J–R** display the parameter covariances over the 15 cardiac cycles.

Table 4
τ_{es} & τ_{ep} RMSE.

Parameter	τ_{es}	τ_{ep}	R_{mv}	Z_{ao}	R_s	C_{sa}	C_{sv}	E_{max}	E_{min}
RMSE $t \leq 8$	0.01	0.009	0.008	0.003	0.2	0.02	2	0.04	0.005
RMSE $t > 8$	0.03	0.02	0.007	0.004	0.06	0.009	4	0.05	0.008

The first row shows the RMSE values of input parameters for $t \leq 8$. The second row displays the RMSE values of the input parameters for $t > 8$ after a continuous perturbation has been applied to E_{min}.

Table 5
E_{min} RMSE.

Parameter	τ_{es}	τ_{ep}	R_{mv}	Z_{ao}	R_s	C_{sa}	C_{sv}	E_{max}	E_{min}
RMSE $t \leq 8$	0.004	0.008	0.007	0.003	0.2	0.01	1	0.03	0.01
RMSE $t > 8$	0.01	0.009	0.009	0.009	0.03	0.008	2	0.03	0.03

The first row shows the RMSE values of input parameters for $t \leq 8$. The second row displays the RMSE values of the input parameters for $t > 8$ after a continuous perturbation has been applied to E_{min}.

$t = 15$. All other input parameters, apart from C_{sv}, tend towards their true values with minimal error after the perturbation is applied to E_{min}. Table 5 indicates that the UKF copes with the perturbation with great efficiency as the RMSE value of the perturbed parameter E_{min} increases minimally. Overall most input parameters do not suffer greatly, with some parameters actually improving there estimation, after the perturbation applied to E_{min}, with only τ_{es} exhibiting a 2.5× increase in error. C_{sv} like in the base state is the input parameter with the largest RMSE error.

3.2.3. C_{sa} & τ_{ep}

In Fig. 8, we see perturbations applied to τ_{ep} and Eq. (15) applied to C_{sa}. Fig. 8B demonstrates the UKF's considerable ability to adapt to differing times which are applied to the end pulse time, τ_{ep}. In Fig. 8F we see that C_{sa} is not found as accurately when the same perturbation is applied to E_{min}, Fig. 7I. Despite C_{sa} not being found as efficiently, the trend of gradual increase is still present in the estimated parameter. We see minimal disruption to other input parameters in the presence of this parameter perturbation case. C_{sv} and R_{mv} appear to diverge from the true parameter estimate. In Table 6 the RMSE values indicate the UKF struggles to capture the perturbation to C_{sa} accurately with a 5× increase in the RMSE. The perturbation applied to τ_{ep} appears to cope well with a minimal increase in the error. Most input parameters appear to improve their estimate of the input parameter value apart from E_{min} where the error increases by 2× and R_{mv} where we see the same increase in the error, however in this case it appears R_{mv} may be diverging. C_{sv} again is the input parameter with the largest RMSE value.

Table 6
C_{sa} & τ_{ep} RMSE.

Parameter	τ_{es}	τ_{ep}	R_{mv}	Z_{ao}	R_s	C_{sa}	C_{sv}	E_{max}	E_{min}
RMSE $t \leq 8$	0.004	0.01	0.009	0.003	0.1	0.02	2	0.03	0.002
RMSE $t > 8$	0.003	0.03	0.02	0.002	0.04	0.1	3	0.007	0.004

The first row shows the RMSE values of input parameters for $t \leq 8$. The second row displays the RMSE values of the input parameters for $t > 8$ after a continuous perturbation has been applied to C_{sa} and discretely we perturb τ_{ep}.

3.2.4. R_s & E_{min}

In this subsection, R_s and E_{min} are perturbed. We see exceptional ability of the UKF to adapt to E_{min} being perturbed by Eq. (15) but R_s fails to track the perturbation as accurately as E_{min}. A majority of input parameters in Fig. 9 converge to the truth value with minimal error apart from R_{mv} and C_{sv}. This parameter perturbation combination causes increases in all parameter variances. The RMSE values displayed in Table 7 indicate once again all none perturbed parameters appear fairly resistant to the changes applied to the input parameter space, we see a 1.67× and 1.25× increase in the RMSE for τ_{es} and τ_{ep}, a 2× increase in the perturbed E_{min} parameter and a 3.33× increase on the RMSE value for Z_{ao}. The perturbed systemic resistance R_s keeps the same level of error before and after the perturbation is applied this is due to R_s failing to accurately find the true parameter value in the first 8 cycles. Then, after the perturbation is applied the R_s estimation fails to track the perturbation to the higher values, $R_s > 1.3$. C_{sv} exhibits the largest values of the RMSE, notably for $t > 8$ we see our smallest

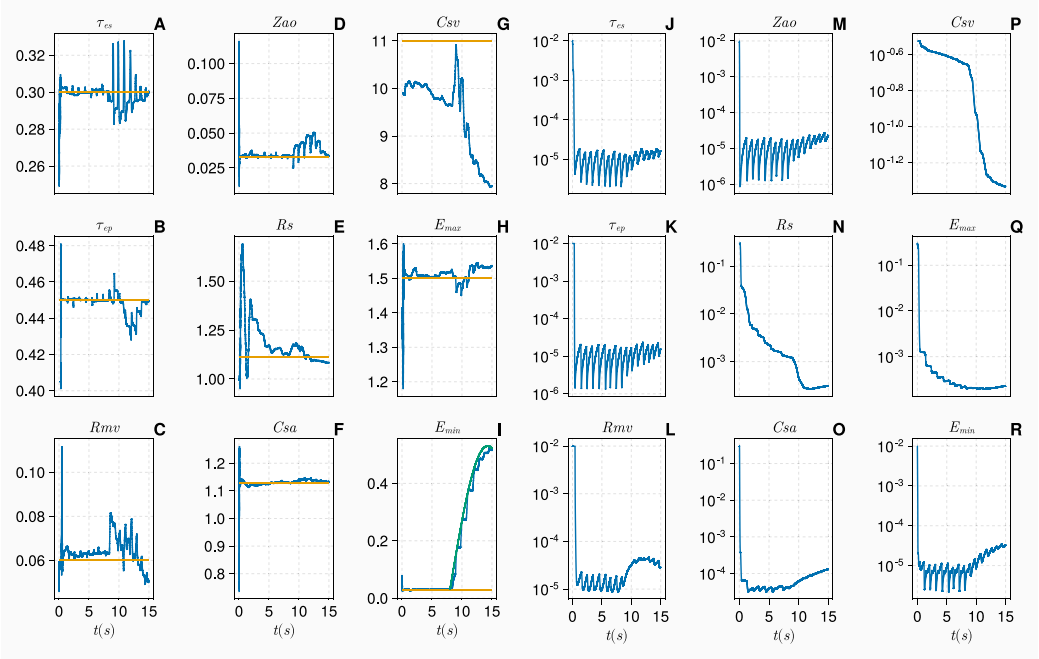

Fig. 7. E_{min} - Figures **A–I** show the parameter estimations over the 15 cardiac cycles with perturbed E_{min}. The yellow, blue and green line represent the true, estimated and perturbed parameter values respectively. Figures **J–R** display the parameter covariances over the 15 cardiac cycles.

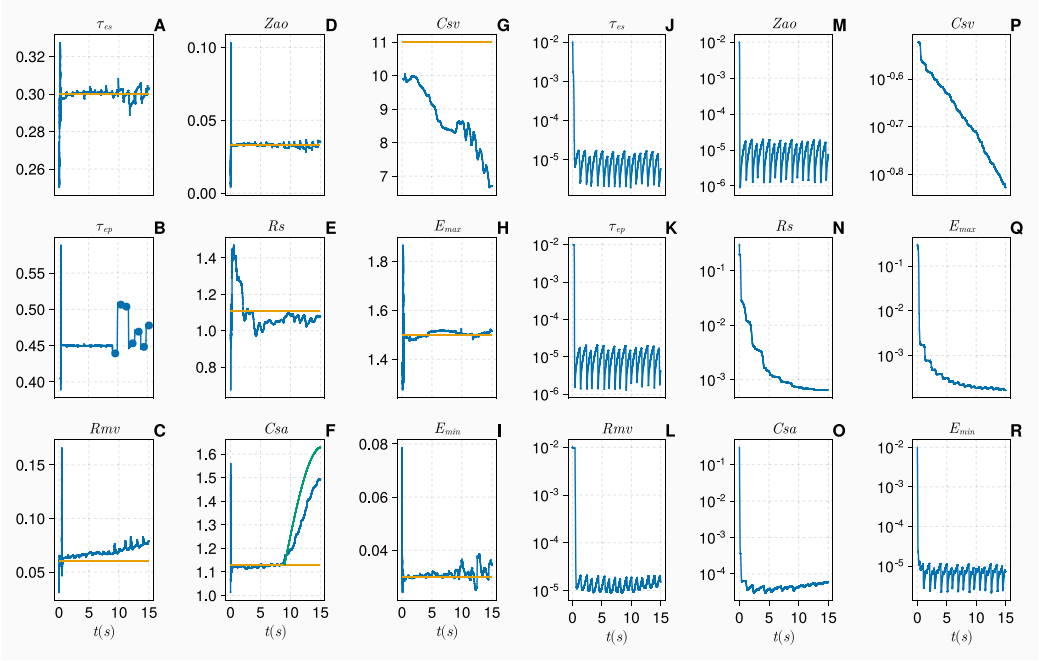

Fig. 8. C_{sa} & τ_{ep} - Figures **A–I** display the parameter estimations over 15 cardiac cycles with perturbed C_{sa} and τ_{ep}. The yellow and blue line represent the true and estimated parameter values respectively. The blue dots and green line represent the perturbed parameter values for τ_{ep} and C_{sa}. Figures **J–R** display the parameter covariances over the 15 cardiac cycles.

value of the RMSE yet for C_{sv}. From Fig. 9G we see C_{sv} appears to tend towards the true value before diverging again.

3.2.5. τ_{es}, τ_{ep} & E_{min}

Fig. 10 shows the outcome after both the timing parameters τ_{es} and τ_{ep} and the minimal contractility parameter E_{min} are perturbed. The timing parameters τ_{es} and τ_{ep} struggle to adapt to the differing timing parameters shown in Figs. 10A and 10B. Perturbing the minimal contractility parameter E_{min} leads to an accurate estimate during every cardiac cycle. We notice the parameter estimates for other input parameters converge with minimal error. C_{sv} diverges from the true value in Fig. 10G. The mitral valve resistance R_{mv} appears to diverge from the true parameter value when the perturbation is applied, but towards the final cardiac cycle it appears to converge back towards the true parameter value. We also notice that the variance appears to increase in all parameters except C_{sv} - see Figs. 10J–R. The above is mirrored in the RMSE values found in Table 8 10 we see a 16.7× and 50× increase in the RMSE value for τ_{es} and τ_{ep}. E_{min} appears robust to

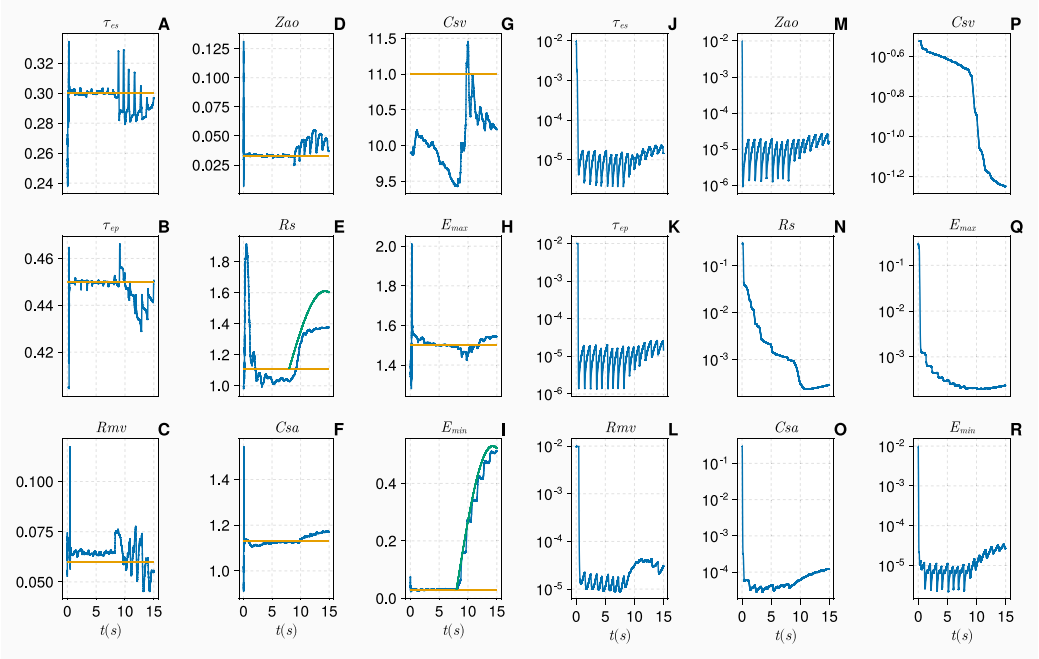

Fig. 9. R_s & E_{min} - Figures **A–I** display the parameter estimations over the 15 cardiac cycles with perturbed E_{min} and R_s. The yellow and blue line represent the true and estimated parameter values respectively. The green lines represent the perturbed input parameter values. Figures **J–R** display the parameter covariances over the 15 cardiac cycles.

Table 7
R_s & E_{min} RMSE.

Parameter	τ_{es}	τ_{ep}	R_{mv}	Z_{ao}	R_s	C_{sa}	C_{sv}	E_{max}	E_{min}
RMSE $t \leq 8$	0.006	0.008	0.007	0.003	0.2	0.02	1	0.04	0.02
RMSE $t > 8$	0.01	0.01	0.008	0.01	0.2	0.03	0.6	0.03	0.04

The first row shows the RMSE values of input parameters for $t \leq 8$. The second row displays the RMSE values of the input parameters for $t > 8$ after a continuous perturbation has been applied to E_{min} and R_s.

Table 8
τ_{es}, τ_{ep} & E_{min} RMSE.

Parameter	τ_{es}	τ_{ep}	R_{mv}	Z_{ao}	R_s	C_{sa}	C_{sv}	E_{max}	E_{min}
RMSE $t \leq 8$	0.006	0.008	0.006	0.003	0.2	0.01	2	0.04	0.04
RMSE $t > 8$	0.1	0.4	0.02	0.005	0.02	0.02	3	0.04	0.04

The first row shows the RMSE values of input parameters for $t \leq 8$. The second row displays the RMSE values of the input parameters for $t > 8$ after a continuous perturbation has been applied to E_{min} and then a discrete perturbation to the timing parameters τ_{es} and τ_{ep}.

the perturbation with the same value of the RMSE being found before and after the perturbation has been applied. All over input parameters suffer from increases to their RMSE value with the exception of the systemic resistance which has a 10× improvement. C_{sv} exhibits the largest RMSE value.

3.2.6. C_{sv}

In this section we perturb the venous compliance parameter C_{sv}. In Fig. 11, we see the parameter estimate diverges from the truth value whist all other parameter estimates in Fig. 11 appear to converge as accurately as in the base state, this is mirrored by constant steady variance. The RMSE values found in Table 9 reflect the accuracy of estimation observed in the base state case, see Table 3. In this case we obtain our smallest value of the RMSE obtained by τ_{ep} after the perturbation was applied to C_{sv}. Table Fig. 11 displays the unanimous trend that as the simulation runs longer the estimation improves, seeming to indicate the perturbation applied to C_{sv} makes no difference

Table 9
C_{sv} RMSE.

Parameter	τ_{es}	τ_{ep}	R_{mv}	Z_{ao}	R_s	C_{sa}	C_{sv}	E_{max}	E_{min}
RMSE $t \leq 8$	0.004	0.008	0.007	0.003	0.09	0.02	2	0.03	0.002
RMSE $t > 8$	0.001	0.0004	0.006	0.0007	0.06	0.003	3	0.008	0.001

The first row shows the RMSE values of input parameters for $t \leq 8$. The second row displays the RMSE values of the input parameters for $t > 8$ after a continuous perturbation has been applied to C_{sv}.

to the estimation of the other input parameters. C_{sv} appears to take no notice of the perturbation and continues to diverge.

4. Discussion

The main investigation of this work was to test the robustness of the UKF in the presence of beat-to-beat variability and physiological parameter perturbations. Overall, we see that the UKF presents itself as a good choice for the identification of input parameters, in terms of accuracy and efficiency. The results in Section 3 demonstrate that all the input parameters exhibit adaptive behaviour, towards their "true" values in the presence of perturbed and non-perturbed input parameters (note: both situations contain synthetic personalised varying cardiac cycle length times). Most remarkably, we see that when certain input parameters are perturbed, namely, the minimal ventricular elastance E_{min} and the ventricle timing parameters τ_{es} and τ_{ep}, the UKF often finds the perturbed values exceptionally well (see Figs. 7 and 6). This provides assurance that, given a similar data set measured in clinic, these parameters are likely to be very accurately estimated, given the same set of clinical measurements are used, given a different set of measurements it is likely the accuracy of the estimations may change for specific input parameters. Other input parameters such as the systemic compliance, C_{sa} and the systemic resistance R_s do not show as accurate estimations (see Figs. 8 and 9). Despite this, one can observe that the general trend of the added perturbation is still present in the estimation of the input parameters.

All cases explored in this work reveal that when a perturbation is applied to a parameter, this normally introduces some disturbance

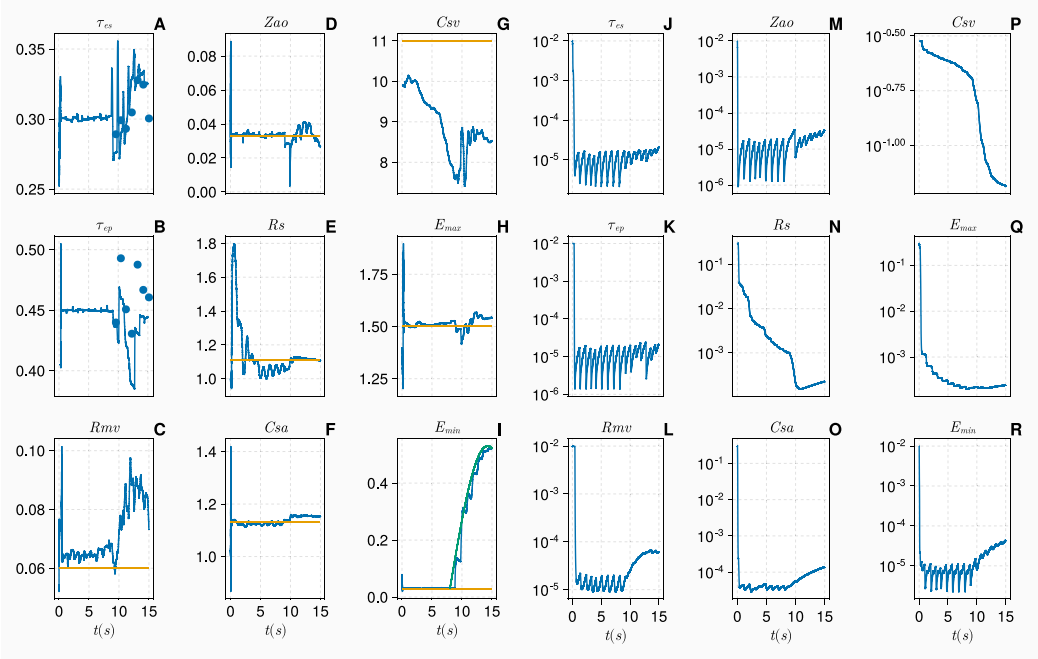

Fig. 10. τ_{es}, τ_{ep} & E_{min} - Figures **A–I** show parameter estimations over 15 cardiac cycles with perturbed timing parameters τ_{es} and τ_{ep} and E_{min}. The yellow and blue line represent the true and estimated parameter values respectively. The blue dots represent the perturbed values of the timing parameters τ_{es} and τ_{ep}. The green line represents the continuous parameter perturbation. Figures **J–R** display the parameter covariances over the 15 cardiac cycles.

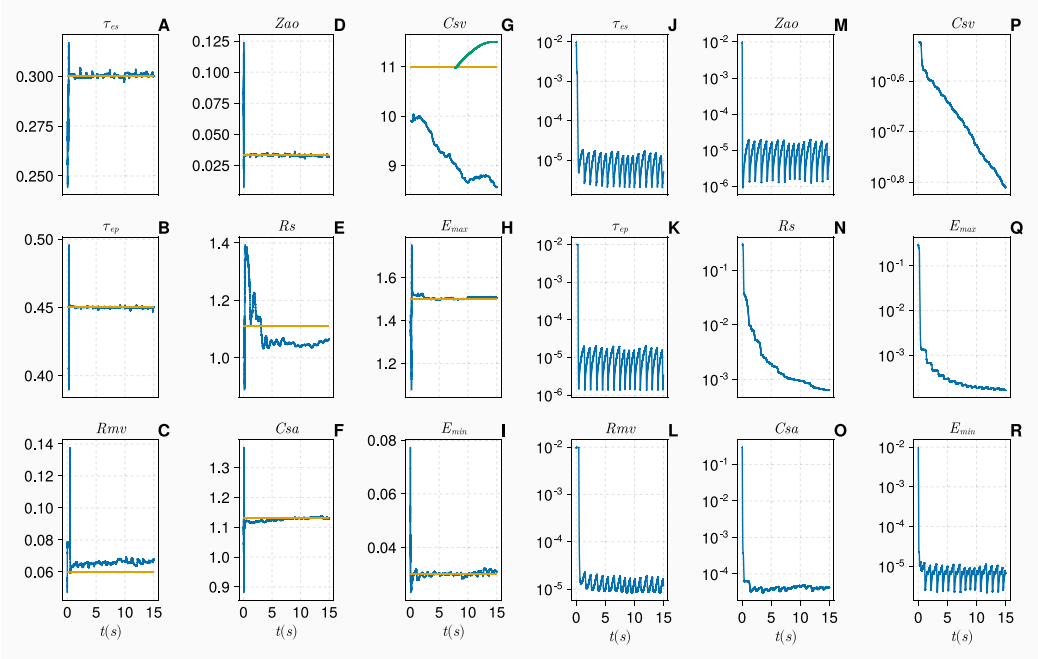

Fig. 11. C_{sv} - Figures **A–I** display the parameter estimations over the 15 cardiac cycles with perturbed E_{min}. The yellow and blue line represent the true and estimated parameter values respectively. The green line represents the perturbed value of C_{sv}. Figures **J–R** display the parameter covariances over the 15 cardiac cycles.

to the other parameter estimations in the model (see the Figures in Section 3) where the disturbance of other parameters in magnitude is often smaller than the magnitude of the perturbed parameter. Further, the disturbance introduced on certain input parameter estimates is a residual effect of another parameter perturbation and not a direct change in a patient's physiological state. The non-perturbed parameter estimations tend towards their true values during a cardiac cycle after a perturbation has been applied. This is evident in the RMSE values, in Section 3. Clinical expertise is essential to ensure that this minimal disturbance can be distilled from true parameter perturbations, for example, in a head-up tilt, one observes a significant drop in systemic resistance before recovery [30]. In Fig. 10, we perturb 3 input parameters and observe the estimations on the timing parameters break down dramatically while the other input parameters appear to be estimated with sufficient accuracy. This is likely to be caused by the 3 parameters being linked by the analytical description of the ventricle in Eq. (6), which highlights the need to identify dependencies and

identifiable parameters before estimation to ensure that accurate and unique parameter estimations can occur.

We examined the continuous sensitivity of input parameters to give an indication on how this may relate to the accuracy of estimation performed by the UKF. The continuous sensitivity analysis (CSA), with results shown in Fig. 5, reveals that most input parameters have a well-defined cycle of importance which correspond to the phases of the cardiac cycle. Two conclusions can be drawn: first, this may explain why most input parameters are estimated with outstanding accuracy, even when their time averaged influence is minimal compared to the most influential parameter τ_{es}. Therefore, the accurate estimation of input parameters is due to either a well-defined cycle of importance or being consistently important. This means the input parameters' effects are observable in the outputs, such that they would be accurately identified by the UKF. The second conclusion from the CSA is what choice of measurements should be made. Often it is the norm to investigate discrete measurements as discussed in Section 2.4. The CSA indicates that there are distinct moments within the cardiac cycle where certain parameters exert a stronger influence compared to at other moments. Our work provides a guide for what one should consider when deciding on which measurements to use to interrogate an input parameter space, i.e., one would choose measurements which are applicable to the time points where all input parameter effects are at their largest and hence improving the chances of making the parameters identifiable.

Notably, two input parameters exhibit potentially surprising results. In the CSA (Fig. 5), we note that the end pulse time, τ_{ep}, exhibits minimal sensitivity across the whole time period investigated. Due to personalised cardiac cycles being included, the effects of end pulse time are truncated. The end pulse time signifies the start of passive filling of the ventricle and due to the passive filling phase of ventricle being cut off from cycle to cycle, this leads to the effects being neglected. Despite the lack of sensitivity, τ_{ep} is found accurately in nearly all cases investigated. One explanation is that the variance of the parameter is consistently low, hence the UKF finds the local minimum estimate and therefore the accurate estimate. Due to this factor, the estimate of τ_{ep} should be considered with more caution than other input parameters.

Within the clinical setting, the end systolic time, τ_{es} is one which is considered to have more impact, as it relates to a QT interval [58,59], which is reflected in the high level of sensitivity seen in Fig. 5. In Section 3, we notice that the estimates of the venous compliance C_{sv} appear to diverge in all cases, despite the well defined CSA curve in Fig. A.12. C_{sv} even diverges in the base state where no parameter perturbations have been applied (see Fig. 4). The variance of the venous compliance is the highest in all parameter estimations, where as the parameters with accurate estimations have steady minimal variances. One explanation for this is that the venous compliance has no direct influence over any of the measurements present in our analysis [60]. As a consequence the parameters effects cannot be observed independently in the synthetic measurements and subsequently the parameter estimate is poor. Despite these special cases, the CSA and UKF results are robust and consistent to all other input parameters.

In the presence of personalised cardiac cycle lengths and parameter perturbations, the average computation time is 90.4 s when executed serially, which corresponds to an average of 6 s per cardiac cycle. If the goal is to implement this approach clinically, it is crucial to reduce the computation time to real-time levels, ensuring a one-to-one relationship between the computational time and the cardiac cycle time. Recent work has shown that a real time implementation without perturbations is available to clinicians [60]. Although the estimations presented in this study demonstrate exceptional accuracy, it is possible to decrease the computational time by reducing the tolerance, complexity of the differential equation solver, and the size of the time step. However, this would inevitably lead to a decrease in the accuracy of the parameter estimate. Currently, there is no existing adaptive time step Kalman filtration approach for this purpose, but its development would significantly enhance the efficiency of the algorithm. Additionally, it would be intriguing to investigate the optimal time step required to ensure sufficient accuracy of the parameter estimate. If either of these points could be developed, it would lead to an increase in the algorithm's efficiency while still maintaining the accuracy level presented within this work.

It is worth noting that the computational expense of this approach is low compared with other computational tools for direct clinical applications [26,61–63]. Even though the computational time of this work does not currently meet real-time requirements, clinicians can still obtain quick insights into a patient's physiological state compared to other tools. Therefore, when pathophysiological conditions are present within the patient data, the UKF should be capable of providing state and parameter estimates that accurately emulate the pathophysiological conditions depicted in the data. The only drawback with this current workflow is that the personalised cardiac cycle lengths must be recorded through an ECG. However, when the pathophysiological condition is not severe, this workflow of collecting personalised cardiac lengths and patient data, feeding them to the UKF, and subsequently interpreting the results to draw medically relevant conclusions, remains an efficient approach to personalised patient-centred care.

One of the primary perturbations employed in this study involves the random scattering of the timing parameters of the elastance function, specifically τ_{es} and τ_{ep}, as defined in Eq. (14). In reality, there exists an unknown function that defines a complex relationship between the length of the cardiac cycle τ, the end systolic time τ_{es}, and the end pulse time τ_{ep}. However, in this work, these parameters are treated as independent parameters of the elastance function. By perturbing τ_{es} and τ_{ep} independently, we are able to demonstrate the robustness associated with the UKF in accurately estimating the timing parameters, even under extreme and unphysiological conditions. hence defining a worst case scenario. This highlights the excellent capability of the UKF to handle perturbations and effectively estimate the timing parameters, despite their independence from the underlying physiological relationships within the cardiac cycle. The other parameter perturbation used (defined in Eq. (15)) applies a steady increase to a parameter value. The results are also tested using a steady decrease in the parameter value and the same conclusions are held. This parameter perturbation is more realistic and similar parameter dynamics have been seen in models which have built-in physics which causes time-varying behaviour of input parameters, such as in models of head-up tilt, microgravity and stochastic versions of the Windkessel model [64–66].

The UKF utilised to estimate input parameters can only do this within a local context. While the UKF excels in providing efficient parameter estimations, there are advanced global optimisation techniques, such as particle filters and genetic algorithms which offer additional benefits such as independence from initial conditions which the UKF can be sensitive to and they are better suited at coping with non-linearity's in the system meaning the global optimisation techniques can often explore a wider input parameter space [67,68]. The employment of carefully chosen sigma vectors to accurately represent a GRV reduces the need for numerical derivative evaluations, which are computationally expensive in global optimisations. UKF's computational advantage is particularly valuable in clinical situations where a decision may present with a time critical aspect. However, relying solely on the UKF's local approach has certain limitations. Since the UKF heavily relies on initial conditions and model assumptions, there is a potential for introducing bias into the estimates.

Within this work, all parameter distributions and initial co-variances were chosen to represent the physiology of the input parameters, as defined in Section 2.5. The dynamical system noise in this work was set to $Q = 10^{-8}$ due to the cardiovascular system's largely deterministic nature and to avoid sigma point collapse, a problem associated with the UKF [26,55]. The measurement noise used in this work was $R =$

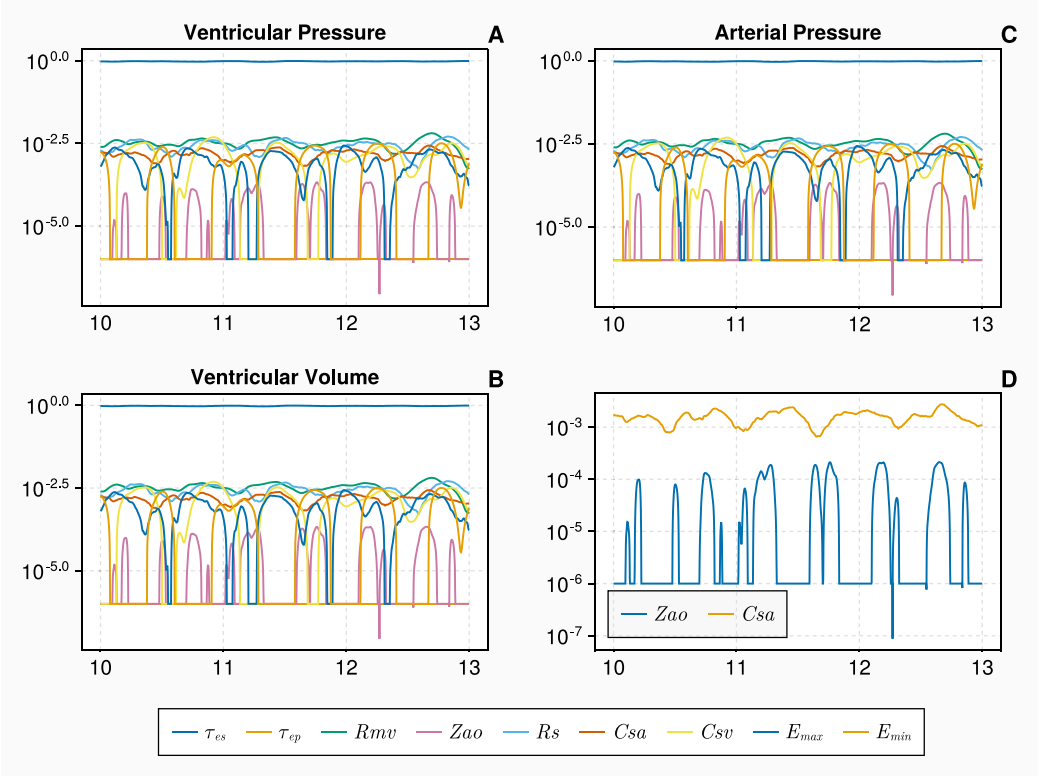

Fig. A.12. Continuous Sensitivity Analysis - Figures **A–C** display the continuous sensitivity with respect to the three measurements investigated in this work. Figure **D** displays continuous sensitivity of Z_{ao} and C_{sa}.

$5^2 \times I_{3\times3}$ to represent the uncertainty within our chosen measurements, as defined in Section 2.3. The local nature of the UKF restricts its ability to explore the entire parameter space, limiting its capability to find the global optimum. In contrast, global optimisation techniques can better navigate multimodal parameter spaces, potentially yielding more accurate estimates.

In the context of cardiovascular clinical decisions, the presence of a subject expert would offer valuable insight. The estimates provided by the UKF can be evaluated by the clinical expert, who possesses specialised knowledge to determine if the estimated parameters align with physiological expectations and accurately represent the patient's physiological state. This evaluation process ensures that the estimates are not only mathematically sound but also relevant from a clinical perspective. By incorporating the expertise of clinical professionals, the UKF's estimates can be validated, enhancing the interpretation of clinical data and providing a more comprehensive assessment of the patient's condition. This collaborative approach between the UKF and the clinical expert fosters an efficient, reliable and clinically relevant decision-making process.

5. Conclusion

We have conducted an analysis of a tractable nine-dimensional single ventricle lumped parameter model, representing the systemic circulation. The lumped parameter approach used in this model is representative of a range of dynamical systems and our observations are in principle applicable to any model — not just a cardiovascular setting. We have developed a novel computational algorithm, designed to incorporate patient-specific beat-to-beat variability into model investigations. Utilising this algorithm, we have efficiently implemented the Unscented Kalman Filter, demonstrating its exceptional adaptability to severe parameter perturbations, representing significant changes in a patient's physiological state.

Our investigation into the computationally efficient, continuous sensitivity of model input parameters has led to a novel explanation for the exceptional capability of the UKF to accurately estimate input parameter values within a single cardiac cycle. This significant insight contributes to our understanding of the UKF's robustness and efficacy. Our research showcases potential clinical applications of the UKF. By utilising patient-specific measurements and employing the close to real-time UKF, it becomes feasible to monitor a patient's physiological state with minimal delay. This novel tool enables medical professionals to promptly identify the onset of a (patho)physiological condition, thus reducing the necessity for invasive procedures and ultimately improving patient care.

Our study contributes to the field of computational science by presenting a representative cardiovascular model, developing an innovative algorithm, elucidating the UKF's remarkable estimation capabilities, and highlighting its potential clinical applications. This research potentially has far-reaching implications for personalised patient monitoring and can lead to substantial improvements in medical care.

Declaration of competing interest

The authors declare that they have no known competing financial interests or personal relationships that could have appeared to influence the work reported in this paper.

Acknowledgements

Harry Saxton is supported by a Sheffield Hallam University Graduate Teaching Assistant Ph.D. scholarship.

Rights retention statement

For the purpose of open access, the authors have applied a Creative Commons Attribution (CC BY) licence to any Author Accepted Manuscript version arising from this submission.

Appendix. Continuous Sensitivity Analysis

See Fig. A.12.

References

[1] R. Gul, Mathematical Modeling and Sensitivity Analysis of Lumped-Parameter Model of the Human Cardiovascular System (Ph.D. thesis), Berlin, 2016.
[2] L. Garber, S. Khodaei, Z. Keshavarz-Motamed, The critical role of lumped parameter models in patient-specific cardiovascular simulations, Arch. Comput. Methods Eng. (2021) 1–24.
[3] F. Regazzoni, M. Salvador, P.C. Africa, M. Fedele, L. Dede, A. Quarteroni, A cardiac electromechanical model coupled with a lumped-parameter model for closed-loop blood circulation, J. Comput. Phys. 457 (2022) 111083.
[4] R.C. Kerckhoffs, M.L. Neal, Q. Gu, J.B. Bassingthwaighte, J.H. Omens, A.D. McCulloch, Coupling of a 3D finite element model of cardiac ventricular mechanics to lumped systems models of the systemic and pulmonic circulation, Ann. Biomed. Eng. 35 (2007) 1–18.
[5] M.J. Colebank, M.U. Qureshi, S. Rajagopal, R.A. Krasuski, M.S. Olufsen, A multiscale model of vascular function in chronic thromboembolic pulmonary hypertension, Am. J. Physiol.-Heart Circul. Physiol. 321 (2) (2021) H318–H338.
[6] M.U. Qureshi, M.J. Colebank, L.M. Paun, L. Ellwein Fix, N. Chesler, M.A. Haider, N.A. Hill, D. Husmeier, M.S. Olufsen, Hemodynamic assessment of pulmonary hypertension in mice: A model-based analysis of the disease mechanism, Biomech. Model. Mechanobiol. 18 (2019) 219–243.
[7] M.A. Bartolo, M.U. Qureshi, M.J. Colebank, N.C. Chesler, M.S. Olufsen, Numerical predictions of shear stress and cyclic stretch in pulmonary hypertension due to left heart failure, Biomech. Model. Mechanobiol. 21 (1) (2022) 363–381.
[8] H. Tang, Z. Dai, M. Wang, B. Guo, S. Wang, J. Wen, T. Li, Lumped-parameter circuit platform for simulating typical cases of pulmonary hypertensions from point of hemodynamics, J. Cardiovasc. Transl. Res. 13 (2020) 826–852.
[9] S. Scarsoglio, A. Guala, C. Camporeale, L. Ridolfi, Impact of atrial fibrillation on the cardiovascular system through a lumped-parameter approach, Med. Biol. Eng. Comput. 52 (2014) 905–920.
[10] S. Pant, C. Corsini, C. Baker, T.-Y. Hsia, G. Pennati, I.E. Vignon-Clementel, A lumped parameter model to study atrioventricular valve regurgitation in stage 1 and changes across stage 2 surgery in single ventricle patients, IEEE Trans. Biomed. Eng. 65 (11) (2018) 2450–2458.
[11] G. Pennati, R. Fumero, Scaling approach to study the changes through the gestation of human fetal cardiac and circulatory behaviors, Ann. Biomed. Eng. 28 (2000) 442–452.
[12] N.D. Williams, R. Brady, S. Gilmore, P. Gremaud, H.T. Tran, J.T. Ottesen, J. Mehlsen, M.S. Olufsen, Cardiovascular dynamics during head-up tilt assessed via pulsatile and non-pulsatile models, J. Math. Biol. 79 (2019) 987–1014.
[13] W. Huberts, S.G. Heinen, N. Zonnebeld, D.A. van den Heuvel, J.-P.P. de Vries, J.H. Tordoir, D.R. Hose, T. Delhaas, F.N. van de Vosse, What is needed to make cardiovascular models suitable for clinical decision support? A viewpoint paper, J. Comput. Sci. 24 (2018) 68–84.
[14] A.A. Baraikan, K. Czechowicz, P.D. Morris, I. Halliday, R.C. Gosling, J.P. Gunn, A.J. Narracott, G. Williams, P. Garg, M. Malawski, et al., Modelling the hemodynamics of Coronary Ischemia, Fluids 8 (5) (2023) 159.
[15] R. Laubscher, J. Van Der Merwe, P. Herbst, J. Liebenberg, Estimation of simulated left ventricle elastance using lumped parameter modelling and gradient-based optimization with forward-mode automatic differentiation based on synthetically generated noninvasive data, J. Biomech. Eng. 145 (2) (2023) 021008.
[16] A.L. Colunga, M.J. Colebank, R. Program, M.S. Olufsen, Parameter inference in a computational model of haemodynamics in pulmonary hypertension, J. R. Soc. Interface 20 (200) (2023) 20220735.
[17] A. Saltelli, M. Ratto, T. Andres, F. Campolongo, J. Cariboni, D. Gatelli, M. Saisana, S. Tarantola, Global Sensitivity Analysis: The Primer, John Wiley & Sons, 2008.
[18] S. Marino, I.B. Hogue, C.J. Ray, D.E. Kirschner, A methodology for performing global uncertainty and sensitivity analysis in systems biology, J. Theoret. Biol. 254 (1) (2008) 178–196, http://dx.doi.org/10.1016/j.jtbi.2008.04.011.
[19] A. Lazarus, D. Dalton, D. Husmeier, H. Gao, Sensitivity analysis and inverse uncertainty quantification for the left ventricular passive mechanics, Biomech. Model. Mechanobiol. 21 (3) (2022) 953–982, http://dx.doi.org/10.1007/s10237-022-01571-8.
[20] S.R. Pope, L.M. Ellwein, C.L. Zapata, V. Novak, C.T. Kelley, M.S. Olufsen, Estimation and identification of parameters in a lumped cerebrovascular model, Math. Biosci. Eng. 6 (1) (2009) 93–115.
[21] H. Saxton, I. Halliday, T. Schenkel, X. Xu, Assessing parameter subset selection methods using a minimalmechanical model of the cardiovascular system, 2023, Available at SSRN 4374559.
[22] N.L. Bjørdalsbakke, J.T. Sturdy, D.R. Hose, L.R. Hellevik, Parameter estimation for closed-loop lumped parameter models of the systemic circulation using synthetic data, Math. Biosci. 343 (2022) 108731.
[23] J.R. Raol, G. Girija, J. Singh, Modelling and Parameter Estimation of Dynamic Systems. Vol. 65, Iet, 2004.
[24] H. Huang, M. Yang, W. Zang, S. Wu, Y. Pang, In vitro identification of four-element Windkessel models based on iterated unscented Kalman filter, IEEE Trans. Biomed. Eng. 58 (9) (2011) 2672–2680.
[25] D. Canuto, J.L. Pantoja, J. Han, E.P. Dutson, J.D. Eldredge, An ensemble Kalman filter approach to parameter estimation for patient-specific cardiovascular flow modeling, Theor. Comput. Fluid Dyn. 34 (2020) 521–544, http://dx.doi.org/10.1007/s00162-020-00530-2.
[26] S. Pant, C. Corsini, C. Baker, T.-Y. Hsia, G. Pennati, I.E. Vignon-Clementel, Inverse problems in reduced order models of cardiovascular haemodynamics: Aspects of data assimilation and heart rate variability, J. R. Soc. Interface 14 (126) (2017) 20160513.
[27] E.A. Wan, R. Van Der Merwe, The unscented Kalman filter, in: Kalman filtering and neural networks, Wiley Online Library, 2001, pp. 221–280, http://dx.doi.org/10.1002/0471221546.ch7.
[28] H.M. Stauss, Heart rate variability, Am. J. Physiol.-Regul. Integr. Comparat. Physiol. 285 (5) (2003) R927–R931.
[29] K. Alcock, Physiological observations of patients admitted from A&E, Nurs. Stand. (through 2013) 16 (34) (2002) 33.
[30] B. Matzuka, J. Mehlsen, H. Tran, M.S. Olufsen, Using Kalman filtering to predict time-varying parameters in a model predicting baroreflex regulation during head-up tilt, IEEE Trans. Biomed. Eng. 62 (8) (2015) 1992–2000.
[31] J. Bezanson, A. Edelman, S. Karpinski, V.B. Shah, Julia: A fresh approach to numerical computing, SIAM Rev. 59 (1) (2017) 65–98, http://dx.doi.org/10.1137/141000671.
[32] C. Rackauckas, Q. Nie, Differentialequations.Jl–a performant and feature-rich ecosystem for solving differential equations in Julia, J. Open Res. Softw. 5 (1) (2017) http://dx.doi.org/10.5334/jors.151.
[33] V.K. Dixit, C. Rackauckas, GlobalSensitivity.jl: Performant and parallel global sensitivity analysis with Julia, J. Open Source Softw. 7 (76) (2022) 4561, http://dx.doi.org/10.21105/joss.04561.
[34] G. Wanner, E. Hairer, Solving Ordinary Differential Equations II. Vol. 375, Springer Berlin Heidelberg New York, 1996.
[35] S. Danisch, J. Krumbiegel, Makie.jl: Flexible high-performance data visualization for Julia, J. Open Source Softw. 6 (65) (2021) 3349, http://dx.doi.org/10.21105/joss.03349.
[36] H. Suga, K. Sagawa, Instantaneous pressure-volume relationships and their ratio in the excised, supported canine left ventricle, Circ. Res. 35 (1) (1974) 117–126.
[37] N. Westerhof, J.-W. Lankhaar, B.E. Westerhof, The arterial Windkessel, Med. Biol. Eng. Comput. 47 (2) (2009) 131–141.
[38] T. Korakianitis, Y. Shi, Numerical simulation of cardiovascular dynamics with healthy and diseased heart valves, J. Biomech. 39 (11) (2006) 1964–1982.
[39] L. Fresiello, G. Ferrari, A. Di Molfetta, K. Zieliński, A. Tzallas, S. Jacobs, M. Darowski, M. Kozarski, B. Meyns, N.S. Katertsidis, et al., A cardiovascular simulator tailored for training and clinical uses, J. Biomed. Inform. 57 (2015) 100–112, http://dx.doi.org/10.1016/j.jbi.2015.07.004.
[40] B. Saugel, K. Kouz, A.S. Meidert, L. Schulte-Uentrop, S. Romagnoli, How to measure blood pressure using an arterial catheter: A systematic 5-step approach, Crit. Care 24 (2020) 1–10, http://dx.doi.org/10.1186/s13054-020-02859-w.
[41] Z. Keshavarz-Motamed, A diagnostic, monitoring, and predictive tool for patients with complex valvular, vascular and ventricular diseases, Sci. Rep. 10 (1) (2020) 1–19, http://dx.doi.org/10.1186/s12968-020-0605-9.
[42] A.M. Mood, Introduction to the Theory of Statistics, McGraw-hill, 1950.
[43] T. Homma, A. Saltelli, Importance measures in global sensitivity analysis of nonlinear models, Reliab. Eng. Syst. Saf. 52 (1) (1996) 1–17.
[44] I.M. Sobol, Global sensitivity indices for nonlinear mathematical models and their Monte Carlo estimates, Math. Comput. Simul. 55 (1–3) (2001) 271–280.
[45] B. Iooss, P. Lemaître, A review on global sensitivity analysis methods, in: Uncertainty Management in Simulation-Optimization of Complex Systems: Algorithms and Applications, Springer, 2015, pp. 101–122.
[46] V. Eck, J. Sturdy, L. Hellevik, Effects of arterial wall models and measurement uncertainties on cardiovascular model predictions, J. Biomech. 50 (2017) 188–194.
[47] M. Asch, M. Bocquet, M. Nodet, Data Assimilation: Methods, Algorithms, and Applications, SIAM, 2016.
[48] S.J. Julier, J.K. Uhlmann, Unscented filtering and nonlinear estimation, Proc. IEEE 92 (3) (2004) 401–422, http://dx.doi.org/10.1109/JPROC.2003.823141.
[49] J. Liepe, S. Filippi, M. Komorowski, M.P. Stumpf, Maximizing the information content of experiments in systems biology, PLoS Comput. Biol. 9 (1) (2013) e1002888, http://dx.doi.org/10.1371/journal.pcbi.1002888.
[50] D. Silk, P.D. Kirk, C.P. Barnes, T. Toni, M.P. Stumpf, Model selection in systems biology depends on experimental design, PLoS Comput. Biol. 10 (6) (2014) e1003650, http://dx.doi.org/10.1371/journal.pcbi.1003650.

[51] S. Pant, C. Corsini, C. Baker, T.-Y. Hsia, G. Pennati, I.E. Vignon-Clementel, M. of Congenital Hearts Alliance (MOCHA) Investigators, et al., Data assimilation and modelling of patient-specific single-ventricle physiology with and without valve regurgitation, J. Biomech. 49 (11) (2016) 2162–2173, http://dx.doi.org/10.1016/j.jbiomech.2015.11.030.

[52] S.J. Julier, The scaled unscented transformation, in: Proceedings of the 2002 American Control Conference (IEEE Cat. No. CH37301). Vol. 6, IEEE, 2002, pp. 4555–4559.

[53] N.J. Higham, Analysis of the cholesky decomposition of a semi-definite matrix, in: Reliable Numerical Computation, Oxford University Press, 1990.

[54] S. Chengode, Left ventricular global systolic function assessment by echocardiography, Ann. Cardiac Anaesthesia 19 (Suppl 1) (2016) S26.

[55] R. Turner, C.E. Rasmussen, Model based learning of sigma points in unscented Kalman filtering, Neurocomputing 80 (2012) 47–53, http://dx.doi.org/10.1016/j.neucom.2011.07.029.

[56] P. Segers, N. Stergiopulos, N. Westerhof, Quantification of the contribution of cardiac and arterial remodeling to hypertension, Hypertension 36 (5) (2000) 760–765.

[57] E.M. Antman, J. Loscalzo, Precision medicine in cardiology, Nat. Rev. Cardiol. 13 (10) (2016) 591–602.

[58] A. Ambhore, S.-G. Teo, A.R.B. Omar, K.-K. Poh, ECG series. Importance of QT interval in clinical practice, Singapore Med. J. 55 (12) (2014) 607.

[59] J. Kautzner, QT interval measurements, Cardiac Electrophysiol. Rev. 6 (2002) 273–277.

[60] H. Saxton, X. Xu, I. Halliday, T. Schenkel, New perspectives on sensitivity and identifiability analysis using the unscented Kalman filter, 2023, arXiv:2306.15710.

[61] D.J. Taylor, J. Feher, K. Czechowicz, I. Halliday, D. Hose, R. Gosling, L. Aubiniere-Robb, M. van't Veer, D.C. Keulards, P. Tonino, et al., Validation of a novel numerical model to predict regionalized blood flow in the Coronary arteries, Eur. Heart J.-Digit. Health 4 (2) (2023) 81–89.

[62] N.L. Bjørdalsbakke, J. Sturdy, E.M. Ingeström, L.R. Hellevik, Monitoring variability in parameter estimates for lumped parameter models of the systemic circulation using longitudinal hemodynamic measurements, BioMed. Eng. OnLine 22 (1) (2023) 34.

[63] E.H. Sepúlveda Oviedo, L.E. Bermeo Clavijo, L.C. Méndez Córdoba, OpenModelica-based virtual simulator for the cardiovascular and respiratory physiology of a neonate, J. Med. Eng. Technol. 46 (3) (2022) 179–197.

[64] K. Buszko, S. Kujawski, J.L. Newton, P. Zalewski, Hemodynamic response to the head-up tilt test in patients with syncope as a predictor of the test outcome: A meta-analysis approach, Front. Physiol. 10 (2019) 184.

[65] C. Basirun, M.L. Ferlazzo, N.R. Howell, G.-J. Liu, R.J. Middleton, B. Martinac, S.A. Narayanan, K. Poole, C. Gentile, J. Chou, Microgravity× radiation: A space mechanobiology approach toward cardiovascular function and disease, Front. Cell Dev. Biol. 9 (2021) 750775.

[66] A.S. Abutaleb, J. Melbin, The estimation of the cardiac time-varying parameters during the ejection phase of the cardiac cycle using the Ito calculus, Cardiovasc. Eng. 10 (2010) 118–127.

[67] S. Katoch, S.S. Chauhan, V. Kumar, A review on genetic algorithm: Past, present, and future, Multimedia Tools Appl. 80 (2021) 8091–8126.

[68] Z. Chen, et al., Bayesian filtering: From Kalman filters to particle filters, and beyond, Statistics 182 (1) (2003) 1–69.